Effect of Sulfur Impurity on Fe(110) Adhesion: A DFT Study

Michelle J. S. Spencer, Ian K. Snook, and Irene Yarovsky*

Applied Physics, School of Applied Sciences, RMIT University, GPO Box 2476V, Melbourne, Victoria 3001, Australia

Received: February 3, 2004; In Final Form: April 27, 2004

The effect of adsorbed S on the adhesion of Fe(110) surfaces is examined using density functional theory. Adsorption of S in the hollow, bridge, and atop sites is modeled at a $^1/_4$ monolayer coverage in match and mismatch interfaces. The calculated adhesion energy curves and fitted universal binding energy relation (Rose et al. *Phys. Rev. B.* **1983**, *28,* 1835) show that the presence of S on the surface reduces the strength of the interface. The effect of adsorbed S on the charge density distribution and magnetic properties of the interface are also examined and can be related to the interfacial geometry. The effect of relaxation of the interfaces at equilibrium is also investigated and is shown to increase the strength of the interface, while reducing the equilibrium interfacial separation.

1. Introduction

The presence of impurities at metal surfaces has been shown to affect their adhesion properties, causing embrittlement or fracture in various metals. One of the most common impurities in Fe is S, and the presence of adsorbed S at Fe interfaces can affect the adhesion, friction, and wear behavior of the metal.[1] The difficulty, however, in examining experimentally the effect of S (or other impurities) on the adhesion properties of Fe lies in the ability to produce clean surfaces free from unwanted impurities that can interfere with the specific contaminant being studied. Using computational methods, the presence or absence of specific impurities can be controlled, allowing information about the structural, electronic, and magnetic properties of the contaminated interface to be obtained.

We have previously examined adhesion between clean bulk-terminated Fe(100), Fe(110),[2] and Fe(111)[3] interfaces in match and mismatch using density functional theory. For Fe(110) surfaces, the matching interface forms the bulk geometry at the equilibrium interfacial separation and is stronger than the mismatching interface.[2] The charge density distribution is shown to be more evenly distributed at equilibrium for both orientations, while regions of low charge density are present for the mismatching interface but not for the matching interface.[4] The magnetic properties of the interfaces can be related to the geometry at the interface. In particular, the magnetic moment enhancement seen for the Fe(110) surface decreases as the matching interface is formed until it reaches zero at the equilibrium separation. In contrast, for the mismatching interface, the enhancement does not reach zero at equilibrium as the bulk structure is not formed.

Adsorption of S on the (110) surface of Fe at the experimentally observed coverage of a $^1/_4$ monolayer has also been examined (ref 5 and references therein). Adsorbed S is found to be stable in atop, bridge, and hollow sites, with the hollow site being most stable.

The effect of a S impurity on Fe adhesion has been examined experimentally[1,6] at various coverages. The S was found to decrease the adhesive strength of the interface compared to the clean surfaces; however, no information was obtained on the structure of the interface or how the S impurity affects the electronic and magnetic properties of the interface.

To compare the relative strength of adhesion between different surfaces, we have previously calculated the adhesion energy values of the interfaces at different interfacial separations. Fitting the universal binding energy relation (UBER)[7] to these values allowed us to obtain the work of separation, W_{sep}, which is defined as the work required to separate an interface to infinity, ignoring relaxation and diffusion processes.[8,9] The equilibrium interfacial separation, d_0, and the screening factor, l, were also obtained. These calculated values allowed us to quantitatively describe the adhesion properties of clean Fe(100), Fe(110), and Fe(111) interfaces and to compare the relative adhesive strength of the interfaces.

In the present study we examine the effect of atomic S on the adhesion of Fe(110) surfaces using density functional theory (DFT) within the plane-wave pseudopotential method. The effect of S adsorbed in three adsorption sites (atop, bridge, and hollow) at a $^1/_4$ monolayer coverage is compared for Fe(110) surfaces in match (epitaxy) and mismatch (out of epitaxy). We examine the calculated adhesion energy curves and changes in electron density distribution and magnetic properties at different interfacial separations. The results are compared to those obtained previously for the clean match and mismatch Fe(110) interfaces.[2,4]

2. Method

2.1. Computational Details. All calculations were performed using the Vienna Ab-initio Simulation Package (VASP),[10−12] which performs fully self-consistent DFT calculations to solve the Kohn−Sham equations.[13] The generalized gradient spin approximation (GGSA), using the functional of Perdew and Wang (PW91),[14] was employed, as previous calculations for bulk iron showed that this approach modeled the bulk features of iron better than the local spin density approximation using the functional of Perdew and Zunger.[15] The electronic wave functions were expanded as linear combinations of plane waves, truncated to include only plane waves with kinetic energies

* To whom correspondence should be addressed. Phone: +61 3 9925 2571. Fax: +61 3 9925 5290. E-mail: irene.yarovsky@rmit.edu.au.

10.1021/jp049506k CCC: $27.50
Published on Web 06/25/2004

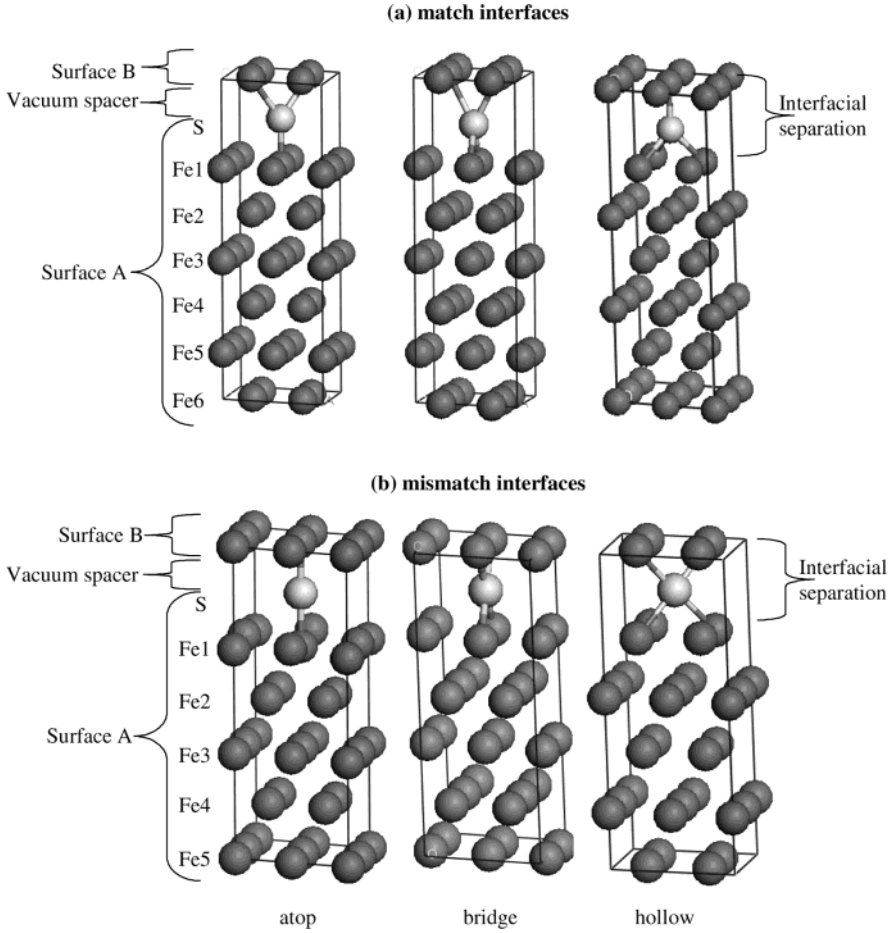

Figure 1. Supercells used to model (a) match and (b) mismatch interfaces with S adsorbed in atop, bridge, and hollow sites. The interfacial separation is modeled by the vacuum spacer. Models shown correspond to the calculated equilibrium separation.

below a cutoff energy (308.76 eV). K-space sampling was performed using the scheme of Monkhorst and Pack[16] using a $6 \times 6 \times 1$ mesh. The ultrasoft pseudopotentials for Fe and S as included in the VASP package[17] were used for all calculations. Our previous work showed this approach to give a good description of bulk, surface, and interfacial properties of Fe,[2−5,18,19] FeS_2,[20−22] and S/Fe(110).[5] For the calculation of fractional occupancies of the relaxed interfaces, a broadening approach by Methfessel−Paxton[23] was used with order $N = 1$ and smearing width 0.1 eV. For accurate calculation of total energies and magnetic moment values of the interfaces at different separations, the tetrahedron scheme[24] was employed, using a Weigner−Seitz radius of 1.3 and 1.164 Å for Fe and S, respectively.

2.2. Interface Models. The Fe interfaces were modeled using the supercell approach, where periodic boundary conditions are applied to the central supercell so that it is reproduced periodically throughout space. Adhesion between a relaxed S/Fe(110) surface and an unrelaxed clean Fe(110) surface was investigated to make a comparison with our previous study of adhesion between unrelaxed clean Fe(110) surfaces.[2] Our previously obtained S/Fe(110) surface models[5] comprised five Fe layers with a S atom adsorbed in an atop, a bridge, or a hollow site on one side of the slab in a $p(2 \times 2)$ arrangement. For the surface relaxation studies, the S and top three Fe layers were relaxed while the bottom two layers were kept fixed. These relaxed models were used in the present study to model a mismatch interface, where insertion of the vacuum spacer in the *z*-direction resulted in formation of the interface. Different interfacial separations were modeled by adjusting the size/thickness of the vacuum spacer. The mismatch interface models are shown in Figure 1 at the equilibrium interfacial separation. Surface A is defined as the relaxed S/Fe(110) surface and surface B as the unrelaxed clean Fe(110) surface. To model matching interfaces, a sixth layer was added to the bottom of the relaxed five-layer model (see Figure 1). Again, the interface is formed by changing the size of the vacuum spacer inserted in the *z*-direction. It should be noted that we define match and mismatch interfaces according to the geometry of the interface formed when the S is removed. The interfacial separation is defined as the distance between the topmost Fe atoms on each surface (see Figure 1). The total energy of each interface was calculated for at least 10 different interfacial separations between 12 and ~2 Å.

The W_{sep} of each interface was determined from a plot of the calculated adhesive energy versus interfacial separation, where the adhesive energy, $E_{ad}(d)$, is obtained as

$$E_{ad}(d) = (E(d) - E(\infty))/A \quad (1)$$

where $E(d)$ is the total energy of the system calculated at interfacial separation d, $E(\infty)$ is the total energy at infinite separation, and A is the cross-sectional area of the interfaces (surface area in the *x*- and *y*-directions). The well depth of this curve at the equilibrium separation, E_0, is equivalent to the work of separation, W_{sep}.[2]

The calculated adhesion energy curves were fitted to the UBER,[7] from which the following parameters were obtained: E_0, the well depth at the equilibrium interfacial separation, d_0; l, the screening length, which for transition metals may be

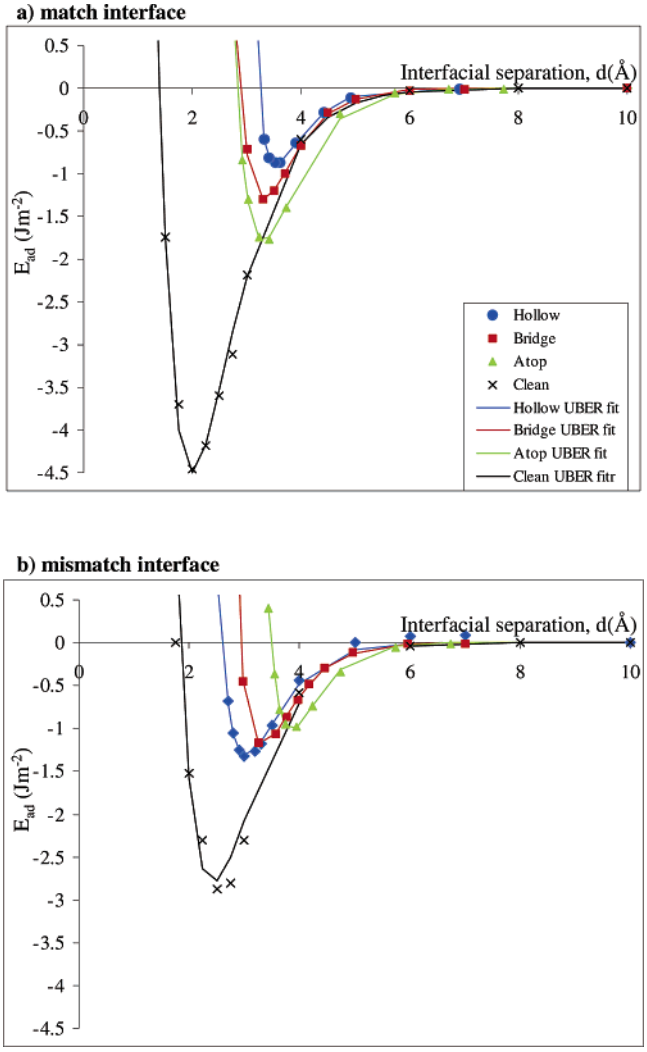

Figure 2. Calculated adhesion and fitted UBER curves for the (a) match and (b) mismatch interfaces with S adsorbed in atop, bridge, and hollow sites. The clean interface data obtained previously[2] are shown for comparison.

interpreted as the surface screening length, i.e., the approximate scale for the distance over which electronic forces can act.

Further calculations were preformed on the interface models at their equilibrium separation, to examine the effect of relaxation on adhesion, electronic, and magnetic properties of the interface. All atoms were allowed to relax in the *x*-, *y*-, and *z*-directions, while also allowing the cell volume to change.

3. Results and Discussion

3.1. Adhesion Energy Curves and UBER Parameters. *3.1.1. Matching Interfaces.* The calculated adhesion energy and fitted UBER curves for S adsorbed in atop, bridge, and hollow sites at match and mismatch interfaces are shown in Figure 2, along with the curves obtained previously for the clean interfaces.[2] The fitted UBER parameters are shown in Table 1.

For the three matching interfaces the S atom lies between two different adsorption sites, one on surface A and the other on surface B. On surface A, the S atom lies above an atop, bridge, or hollow site, while on surface B, the S atom lies above a hollow, bridge, or atop site, respectively. For the bridge−site interface, the two Fe atoms forming the bridge site on surface B are oriented at right angles to those forming the bridge site on surface A. The topmost Fe atoms on surface A are relaxed and show some buckling due to the adsorption of S on the surface as shown previously.[5] The Fe atoms on surface B represent a clean bulk-terminated surface. The interfaces are described as atop, bridge, or hollow, depending on the site in which the S atom is adsorbed on surface A.

TABLE 1: Calculated UBER Parameters for the S-Contaminated Match and Mismatch Interfaces as Well as Those Obtained Previously[2] for the Corresponding Clean Interfaces[a]

site	$E_0 = W_{sep}$ (E_{ad}) (Jm^{-2})	d_0 (Å)	l (Å)	R^2
	Match Interface			
atop	1.79 (2.41)	3.30 (2.30)	0.47	0.998
bridge	1.30 (1.95)	3.30 (2.25)	0.43	0.998
hollow	0.88 (1.50)	3.55 (2.29)	0.37	1.000
clean[2]	4.494	1.991	0.590	0.99
	Mismatch Interface			
atop	1.02 (1.16)	3.86 (3.10)	0.37	0.999
bridge	1.19 (1.42)	3.33 (2.78)	0.43	1.000
hollow	1.32 (1.72)	3.03 (2.60)	0.45	0.995
clean[2]	2.795	2.427	0.588	0.99

[a] The calculated adhesion energy (E_{ad}) and d_0 values for the relaxed S-contaminated interfaces are shown in parentheses.

The high R^2 values (Table 1) for all the fitted UBER curves (>0.99) indicate that the UBER provides a good description of adhesion between S-contaminated Fe(110) surfaces.

From Table 1 and Figure 2, for the match interface, the presence of S can be seen to significantly decrease the calculated work of separation, W_{sep}, as compared to the clean interface, with a reduction of 80%, 71%, and 60% for the hollow, bridge, and atop sites, respectively. Even though S reduces the adhesive strength of the clean interface, the adhesion is strongest when S is adsorbed in an atop site, of all contaminated surfaces.

According to the geometry of the atop and hollow interfaces, they should be almost identical; however, the calculated W_{sep} for the atop site interface is more than twice as large as that for the hollow site interface. This difference arises from the difference in energy of the S adsorbed on the isolated surfaces. The adhesion energy is calculated by subtracting the energy of the interface at infinite separation from the energy of the surfaces at a particular separation. At equilibrium, where the adhesion energy is at a minimum, the total energies of the atop and hollow site interfaces only differ by <0.007%. At infinite separation, the total energies, however, are not the same because the separated surfaces are different. The clean surface is identical in both cases, but S is adsorbed in an atop site on one surface and in a hollow site on the other. As shown previously, the hollow site is more stable than the atop site;[5] hence, the calculated adhesion energy is lower for the atop interface.

The equilibrium interfacial separation values, d_0, of the S-contaminated interfaces (Table 1) are larger than those for the corresponding clean interface as expected, because the presence of adsorbed S prevents the Fe surfaces from getting as close to each other as in the clean interface.

At the equilibrium separation, the distance of the S atom from surface A or B is found to be almost the same for identical adsorption sites. That is, on surface A (as shown previously[5]) S lies 2.06, 1.7, and 1.49 Å above the atop, bridge, and hollow sites, respectively. On surface B, the S is calculated to sit 1.51, 1.69, and 2.07 Å above the hollow, bridge, and atop sites, respectively, giving distances almost identical to those from surface A. The small differences can be attributed to the fact that surface A is relaxed, while surface B is not. This is also why the addition of the distances of S from surfaces A and B do not exactly equal the d_0 values, and explains the small difference between the atop and hollow interface d_0 values.

Similar to W_{sep}, the screening length, l (Table 1), is also reduced compared to that of the clean interface, by 20%, 27%, and 37% for the hollow, bridge, and atop interfaces, respectively. This reduction in the screening length indicates that the attraction between the contaminated surfaces occurs over a shorter separation distance compared to that between the clean surfaces. The relative order of the l values can be correlated to the distance of the S atom from the underlying surface, where the distance is greatest for the atop site but smallest for the hollow site. Hence, as the surfaces approach each other, the clean surface (B) begins to interact with the S-contaminated surface (A) sooner for the atop site as the S sits further from surface A than it does for the other two sites.

Despite the l values being smaller for the S-contaminated interface, it can be seen from the adhesion energy curve (Figure 2) that, at separations from 6 to ~3.5 Å, the attraction between surfaces with S adsorbed in the atop site is stronger than between the clean surfaces. This is not the case for the bridge or hollow sites, which show adhesion energy values very similar to that of the clean interface at this separation range. Hence, if S is present on the Fe(110) surface in the atop site, it is more likely to adhere, even though the resulting interface will be weaker than the corresponding clean one, as evidenced by the respective W_{sep} values.

By definition, W_{sep} corresponds to the energy required to separate the surfaces to infinity disregarding the effect of plastic or diffusional processes. To remove some of the constraints applied to our interface models and to examine the effect of relaxation of the interface at equilibrium, further calculations were performed that allowed all S and Fe atoms to relax, while also allowing the cell volume to change. The calculated adhesion energy of the relaxed interfaces is therefore a better approximation of the work of adhesion.

The adhesion energy values shown in Table 1 for the relaxed interfaces indicate that the adhesion energy for all interfaces increases. The relative order remains the same as before relaxation; however, the difference in values between the relaxed atop and hollow site interfaces is reduced to 10% as some of the constraints applied previously to the surfaces are removed and the energy of the interface is lowered. However, the remaining difference in adhesion energy values still arises mostly from the different stabilities of the isolated surfaces.

The geometry of the matching interfaces also changed slightly after relaxation, with all interfaces relaxing so as to reduce the interfacial separation (Table 1). The atop and hollow sites both gave a relaxed separation of ~2.3 Å, with the bridge site interfacial separation decreasing to 2.25 Å. In addition, the S−Fe nearest neighbor distances were found to decrease to 1.98, 2.04, and 2.03 Å for the atop, bridge, and hollow sites, respectively, as compared to 2.09, 2.15, and 2.19 Å for the isolated surfaces.[5] These distances may be shorter than for the isolated surfaces because of the stronger attraction between the Fe atoms across the interface at this separation, which reduces the S−Fe distance so as to bring the two surfaces closer together. The topmost atoms on both surfaces also showed a buckling as seen on the isolated S-adsorbed surface, with the buckling of the Fe atoms not directly bonded to the S atom being greater than on the isolated surface.

These S−Fe bond distances for the different matching interfaces are similar to those found for iron sulfide minerals, such as pyrite (FeS_2), marcasite (FeS_2), and pyrrhotite ($Fe_{1-x}S$, where $0 < x < 0.2$). While both pyrite and marcasite have an FeS_2 stoichiometry, they have different crystal structures, with pyrite being cubic and marcasite being orthorhombic. The slightly different structures give rise to S−Fe bond distances that are very similar. In pyrite, the S−Fe bond distance has been determined to be 2.259 Å,[25] while in marcasite, the S−Fe distance is 2.213 or 2.243 Å.[26] For pyrrhotite, which exists in a hexagonal or monoclinic form, the S−Fe distances are in the range 2.37−2.72 Å (ref 27 and references therein). The similarity of the S−Fe distances to our values indicates that similar bonding occurs and that chemical bonds are formed after adhesion of the S-contaminated Fe(110) surfaces. Our distances are all slightly smaller than these values as the stoichiometry of the interfaces, as well as the coordination number of the S and Fe atoms, is different from those of the above structures. It will be interesting to compare the values for different S coverages where the stoichiometry and coordination number may more closely match that of the naturally occurring iron sulfide structures. This will be the subject of future work.

3.1.2. Mismatching Interfaces. For the mismatch interfaces, the Fe atoms are arranged symmetrically about the S atom, with the S atom sitting between two atop sites, two bridge sites, or two hollow sites.

As seen from Table 1, the presence of adsorbed S at the interface again reduces W_{sep}, compared to that of the clean interface. The amount it is reduced, however, is smaller than for the corresponding matching interfaces, W_{sep} being 53%, 57%, and 63% smaller than the W_{sep} of the clean interface for S adsorbed in the hollow, bridge, and atop sites, respectively.

Similar to the clean interfaces, the mismatch interface is generally weaker than the match interface, except for the hollow mismatch interface, which is actually stronger than the hollow matching interface, indicating the presence of adsorbed S stabilizes the interface more in a mismatch alignment. The mismatching interface, however, is still not as strong as the atop matching interface.

The d_0 values of the S-contaminated mismatch interfaces (Table 1) are again larger than those for the clean interface as S prevents the Fe surfaces from getting as close to each other. The distance of S from surface B is almost the same as that from surface A for all interfaces as the Fe atoms are arranged symmetrically about the S atom, with the small differences resulting because surface A is relaxed while surface B is unrelaxed. The equilibrium interfacial separation is therefore as expected, largest for the atop interface, followed by the bridge and then the hollow interfaces, as the distance of S from the surface decreases from the atop, to the bridge, and then to the hollow site.[5]

Comparison of the matching and mismatching d_0 shows that their relative values can also be explained by the S adsorption geometry at the equilibrium separation, where d_0 for the mismatching atop interface is largest as the S atom lies directly between two Fe atoms, and smallest for the mismatching hollow interface where S lies between two hollow sites at the interface.

The presence of S again reduces the calculated l values (Table 1); however, they are similar to those of the matching interface, with the bridge matching and mismatching interfaces being identical, the hollow match and atop mismatch interfaces being identical, and the atop match and hollow mismatch being only 0.02 Å different, all in line with the geometry of surface B that approaches that of surface A. It appears that the stronger interfaces have a slightly larger l value.

Relaxation of the mismatching interfaces at their equilibrium separations showed changes similar to those seen after relaxation of the matching interfaces. The E_{ad} values for the atop, bridge, and hollow mismatching interfaces (Table 1) all increase, while keeping the same relative order as before relaxation. The relaxed

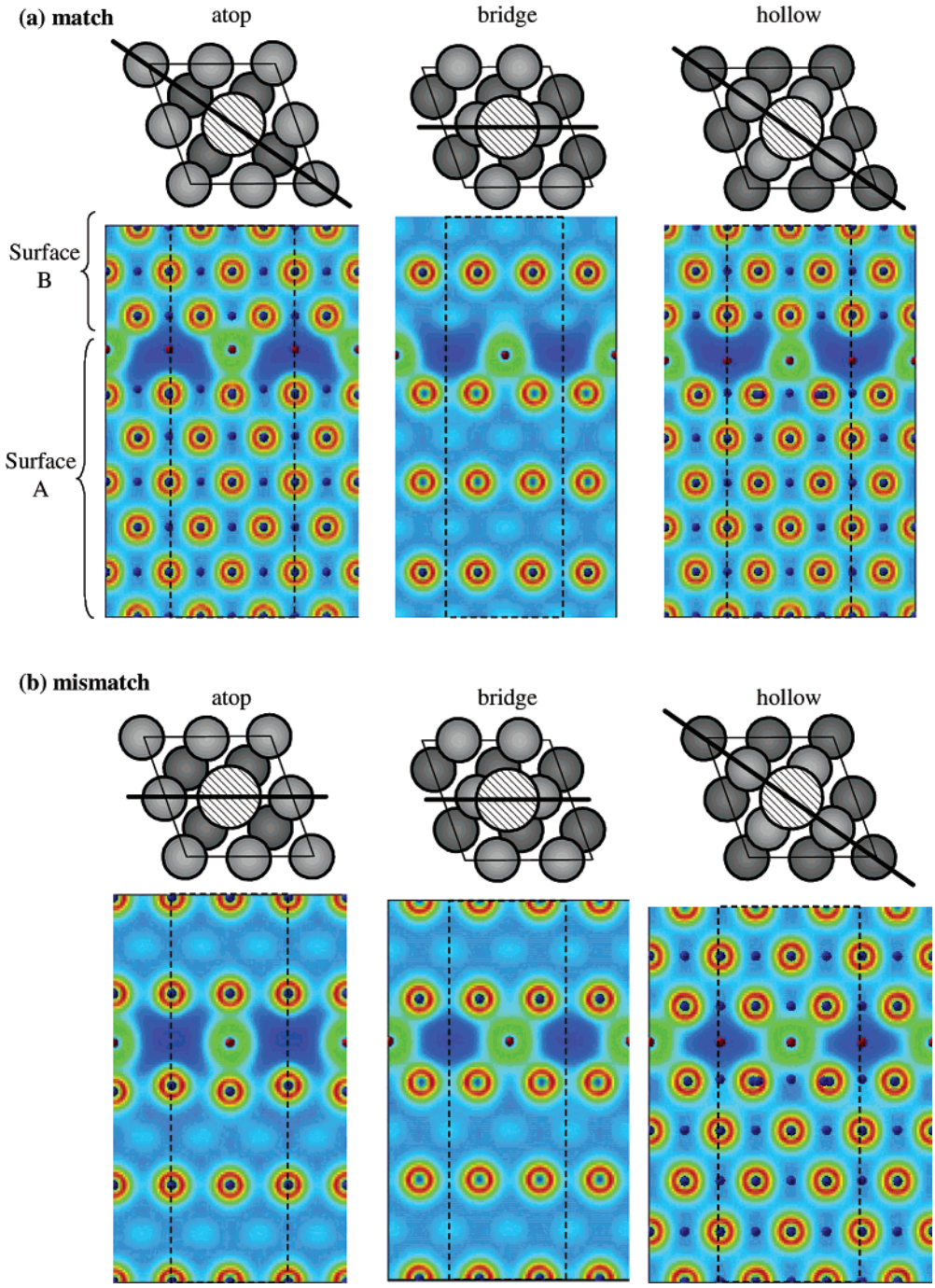

Figure 3. Charge density plots of the (a) match and (b) mismatch interfaces with S adsorbed in atop, bridge, and hollow sites. The slices were taken along the azimuth indicated on the surface model. The central supercell is indicated by the dashed line.

d_0 values (Table 1) are again smaller than those of the unrelaxed interfaces. They are also still larger than those of the relaxed matching interfaces as more surface Fe atoms are bonded directly to the S atom for the mismatching interfaces and hence there is not as strong an attraction between the nonbonded Fe atoms to bring the surfaces closer together. Similar to the matching interfaces, there is a buckling of surface B after relaxation. The Fe atoms on surface A also relax further, so the buckling is more pronounced than on the isolated surface and almost the same as on surface B, resulting in an interface that is geometrically symmetric.

Similar to the matching interfaces, the S−Fe distances decrease slightly after relaxation, becoming 1.97, 2.13, and 2.15 Å for the atop, bridge, and hollow interfaces, as opposed to 2.09, 2.15, and 2.19 Å for the isolated surfaces.[5] The distances of the S atom to the closest Fe atom on surfaces A and B are the same, as expected, because the interfaces are symmetrical about the S atom. For the bridge and hollow sites, the S−Fe distances do not shorten as much as for the matching interface. This may be due to the fact that S is more highly coordinated for these interfaces. Again, the lengths of the S−Fe bonds indicate that chemical bonding occurs across the interface.

3.2. Charge Density. *3.2.1. Matching Interfaces.* The charge density plots for the match interfaces at equilibrium separation are shown in Figure 3. The charge density slices are taken along the direction that cuts through the S atom and the Fe atoms on surfaces A and B that are closest to the S atom.

At the equilibrium separation for all match interfaces the S atom remains bonded to the same Fe atoms as on the isolated surface.[5] That is, for the atop site, the S atom is bonded to the

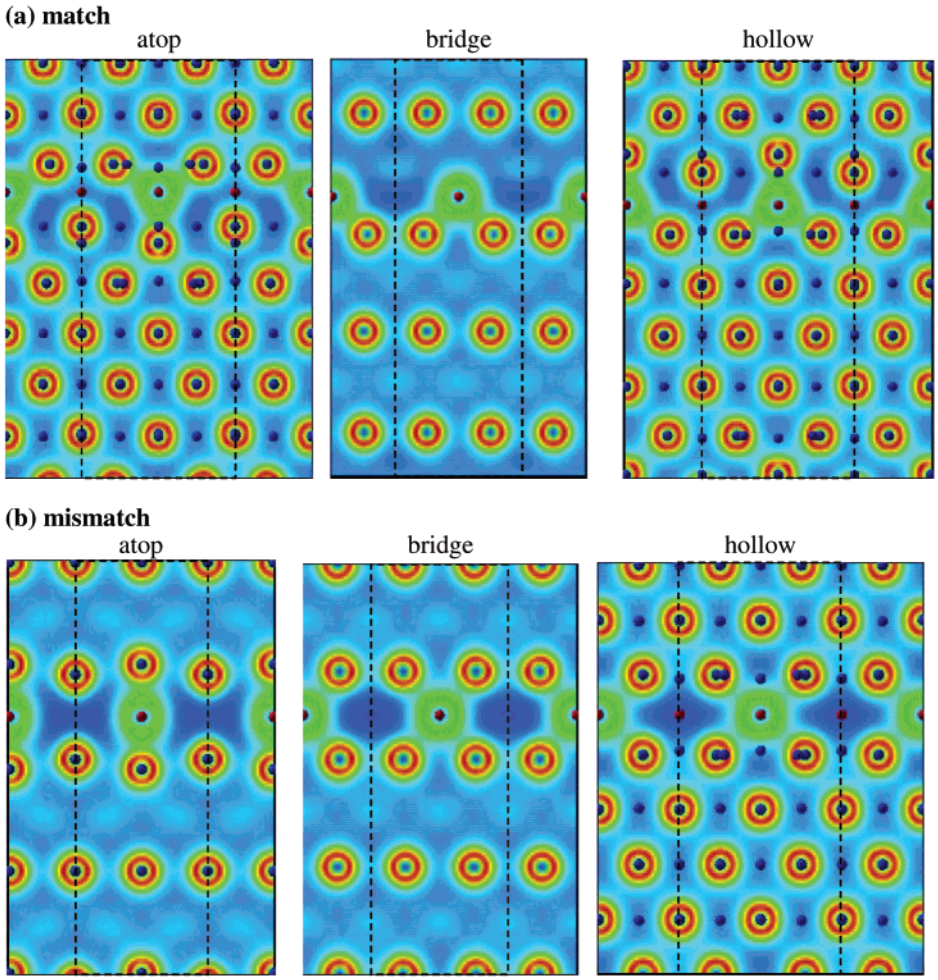

Figure 4. Charge density plots of S-contaminated atop, bridge, and hollow (a) matching and (b) mismatching interfaces at equilibrium, after relaxation of atomic positions and cell volume. The central supercell is indicated by the dashed line.

Fe atom directly below it. For the bridge site it is bonded to the two closest surface Fe atoms. For the hollow site it is more strongly bonded to two of the four surface Fe atoms, as these two atoms are closer to the S atom than the other two.

As expected, when surface B is brought in contact with surface A to form the interface, the charge density plots show bonding occurring between the S atom and the Fe atoms on surface B.

For the atop interface there is an increase in charge density between the S atom and two of the surface Fe atoms on surface B that form the hollow site, indicating the S atom is tribonded at the interface.

For the bridge interface, there appears to be no increase in charge density between the S atom and the Fe atoms on surface B; however, a slice taken perpendicular to the one shown indicates an increase in charge density between the S atom and the two Fe atoms on surface B that lie perpendicular to the bonded atoms on surface A. This is more clearly seen in Figure 1, which shows the geometry of the interface at equilibrium and the four Fe atoms that the S atom is directly bonded to.

For the hollow interface, there is a concentration of charge density between the S atom and the Fe atom on surface B that lies directly above it, in line with the interfacial geometry which shows S bonding in an atop site on surface B.

For all interfaces there are regions of low charge density between the S atoms which were not seen for the clean interface as the S atom prevents the Fe atoms from getting close enough to interact strongly.

After relaxation of the interfaces at equilibrium separation, the charge density plots show significant changes (Figure 4). For all interfaces, the large regions of low charge density are reduced as the surface Fe atoms that are not directly bonded to the S atom move closer to each other to redistribute the charge more evenly at the interface. The atop and hollow interface charge density plots also look identical, reflecting the changes indicated by the geometry analysis after relaxation.

3.2.2. Mismatching Interfaces. For the mismatch interfaces, the charge density plots (Figure 3) show symmetrical bonding about the S atom in line with the geometry of the interface.

For the atop interface, there is a concentration of charge density between the S atom and the Fe atoms directly above and below it. For the bridge and hollow interfaces, the S atom is bonded to four Fe atoms within the same plane, as indicated by the increase in charge density between the S atom and the two Fe atoms on surface A and two on surface B. The Fe atoms, however, are closer to the S atom for the bridge site than for the hollow site.

Similar to the matching interfaces, there are again large regions of low charge density at the interface between adjacent S atoms, as the S atom prevents the Fe surfaces from getting closer to each other. These regions of low charge density were also seen for the clean mismatching interface,[4] where there was a concentration of high charge density between the topmost Fe atoms on each surface that were directly facing each other but a lack of charge density between these atoms. For the atop interface, in particular, there are surface Fe atoms on surfaces

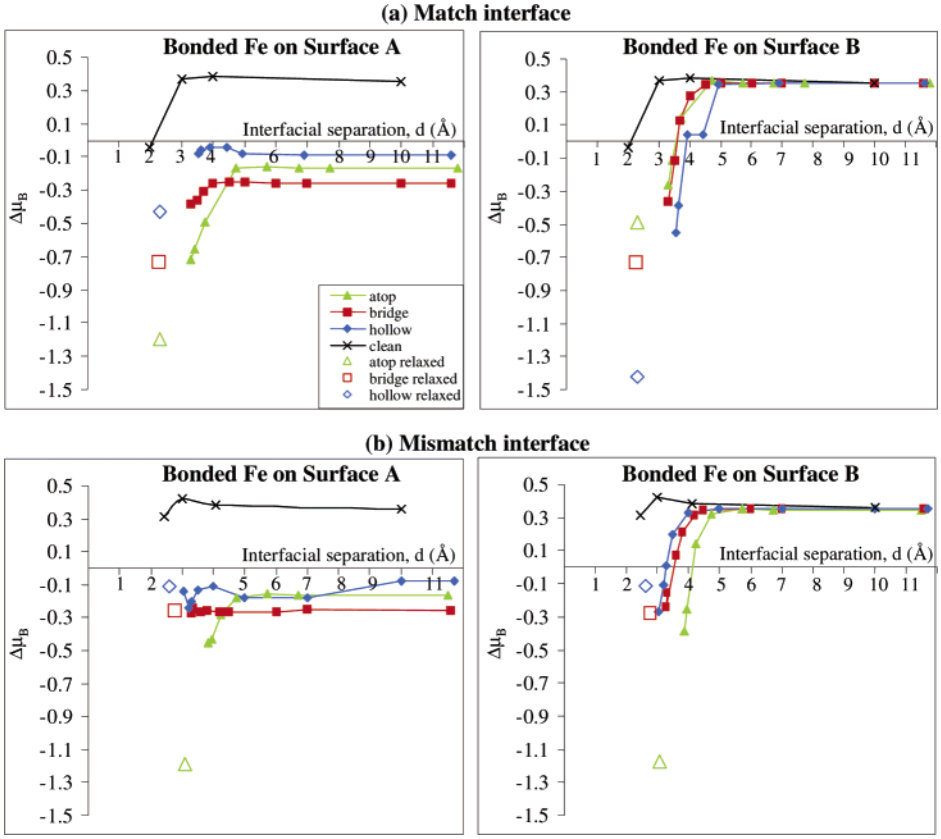

Figure 5. Magnetic moment enhancements for the Fe atoms on surfaces A and B that are closest to the S atom adsorbed in atop, bridge, and hollow sites in (a) match and (b) mismatch interfaces. The clean interface values obtained previously[4] are shown for comparison. The magnetic moment enhancements of the S-contaminated interfaces at equilibrium, after relaxation of the atomic positions and cell volume, are shown as open symbols.

A and B not directly involved in bonding to the S atom that directly face each other; however, as they cannot get close enough there is no substantial increase in charge density between them. These low charge density regions give rise to a weaker interface and explain the reduction in the calculated W_{sep} values as compared to those of the matching interface.

After relaxation (Figure 4), however, the topmost atoms on surfaces A and B move so as to redistribute the charge more evenly at the interface, and the regions of low charge density are reduced. They are, however, still present and larger than for the corresponding matching interfaces, as reflected by the relative strength of the interfaces.

The changes in the charge density distribution indicated by the plots in Figures 3 and 4 for both matching and mismatching interfaces at equilibrium separation further support the chemical, as opposed to physical, nature of the bonds formed at the interface.

3.3. Magnetic Moments. The magnetic moment enhancements, $\Delta\mu_B$, were calculated as a function of interfacial separation for the Fe atoms on surfaces A and B that are most strongly bonded to the S atom (as indicated by the charge density plots and shown bonded to the S in Figure 1). The enhancements are determined by subtracting the previously calculated μ_B value of 2.40 μ_B for bulk Fe[4] from the μ_B of the topmost surface Fe atoms and are shown for the match and mismatch interfaces in Figure 5.

3.3.1. Matching Interfaces. At a separation of 12 Å, the $\Delta\mu_B$ values of atoms on surface A are negative for all adsorption sites, in line with the values calculated previously for the isolated S-contaminated surface, where S reduced the surface Fe layer magnetic moment values below that of the bulk.[5] On surface B, the Fe $\Delta\mu_B$ values are positive for all interfaces, in line with the enhancement seen for clean bulk-terminated Fe(110) surfaces and also shown for the clean Fe(110) interface at the same separation.[4] The agreement between these values and those of the isolated surfaces is in line with the calculated adhesion energy curves, which show that there are no attractive forces acting between surfaces A and B at this separation.

As the interfacial separation is reduced, the $\Delta\mu_B$ values of atoms on surface A change little until below ~5 Å, where the atop and bridge site $\Delta\mu_B$ values decrease significantly at equilibrium to −0.7 and −0.4 μ_B, respectively. In contrast, the hollow site values increase slightly before decreasing to a value of approximately −0.1 μ_B. Hence, at equilibrium the $\Delta\mu_B$ is largest for the hollow site, followed by the bridge and then atop sites. This order may be related to the change in coordination of the S atom upon formation of the interface. For the atop site it is only singly coordinated to surface A at 12 Å; however, at the equilibrium separation, it becomes doubly coordinated to surface B. Hence, the coordination has tripled from what it was at the isolated surface. For the bridge site, the coordination doubles, while for the hollow site is increases 1.5 times. Hence, the increase in coordination appears to be related to the change in $\Delta\mu_B$ at equilibrium, where more spin pairing may occur with a larger change in coordination.

Similar to surface A, the μ_B values of atoms on surface B change little until an interfacial separation around 5 Å, where the $\Delta\mu_B$ values decrease significantly due to interaction of the surfaces at this separation. The μ_B enhancement becomes negative for all sites at the equilibrium separation and is smaller for the hollow site, followed by the bridge and atop sites. This order is opposite to that seen for surface A as the increase in

coordination of the S atom is in the order opposite to that seen for surface A.

In addition, it would be expected that the atoms in similar bonding arrangements would have similar magnetic moment values and hence enhancements. Indeed, the $\Delta\mu_B$ values for the bridge interface are very similar, while the values for the atop and hollow interfaces are close but not identical due to the small differences between the relaxed and unrelaxed surfaces.

The $\Delta\mu_B$ values for the interfaces at equilibrium after relaxation are shown in Figure 5. The $\Delta\mu_B$ values all become more negative as the interfacial separation decreases and the surface Fe atoms across the interface interact more strongly with each other, causing spin pairing and a reduction in the magnetic moment. The magnetic moment enhancements for the bridge site atoms on surfaces A and B become identical. The atop and hollow site values also become equal, consistent with the change in geometry of the atoms at the interface.

3.3.2. Mismatching Interfaces. For the mismatch interfaces, the $\Delta\mu_B$ values are the same as for the match interface at 12 Å as there is no interaction between the surfaces at this separation. The general trend of the values at smaller separations is the same as for the matching interfaces; however, the $\Delta\mu_B$ values remain positive at all separations including equilibrium. As the interface is symmetrical about the S atom, the $\Delta\mu_B$ values of the Fe atoms on surfaces A and B are expected to be the same; however, there are small differences, particularly for the hollow site as surface B is not relaxed. After relaxation, the $\Delta\mu_B$ values become identical, indicating the bonding is symmetrical at the interface. The values are also in the same order as on the isolated surfaces as the increase in S−Fe coordination is in the same order, with the S atom being least coordinated in an atop site on the surface or at the interface and most highly coordinated on the hollow site on the surface as well as at the interface.

4. Conclusion

The effect of adsorbed S at matching and mismatching Fe(110) interfaces (in atop, bridge, and hollow sites) has been examined, showing that the presence of adsorbed S decreases the adhesion as compared to that of the clean interfaces. The interface is strongest when S is adsorbed in an atop site at a matching interface. The atop and bridge matching interfaces are both stronger than the corresponding mismatch interfaces; however, the hollow mismatch interface is stronger than the match interface. This difference is related to the interfacial geometry.

Adsorbed S increases the equilibrium interfacial separation, as S prevents the Fe surfaces from getting as close to each other. The calculated equilibrium separation values are directly related to the distance of S adsorbed in atop, bridge, and hollow sites on isolated Fe(110) surfaces, with the hollow mismatching interface having the smallest separation as S bonds to two hollow sites at equilibrium.

The charge density plots correlate with the geometry of the S and Fe atoms at each interface, showing S bonds to the closest Fe atoms on each surface forming the interface, and at equilibrium the most uniform density distribution is observed. These changes, along with the resulting S−Fe bond distances at equilibrium separation, indicate that chemical bond formation occurs across the interfaces. Likewise, the magnetic properties can be shown to be related to the change in coordination of the S atom upon formation of the interface and the related charge density distribution changes.

Relaxation of the interfaces at the equilibrium separation results in a decrease in the interfacial separation and an increase in the strength of the interface. A buckling of the topmost Fe layers of each surface forming the interface occurs, such that nonbonded Fe atoms move so as to reduce the interfacial separation and to redistribute the charge more evenly at the interface.

Acknowledgment. The Victorian Partnership for Advanced Computing (VPAC) and Australian Partnership for Advanced Computing (APAC) are acknowledged for provision of computer facilities.

References and Notes

(1) Hartweck, W.; Grabke, H. J. *Surf. Sci.* **1979**, *89*, 174.
(2) Hung, A.; Yarovsky, I.; Muscat, J.; Russo, S.; Snook, I.; Watts, R. O. *Surf. Sci.* **2002**, *501*, 261.
(3) Spencer, M. J. S.; Hung, A.; Snook, I. K.; Yarovsky, I. *Surf. Sci.* **2002**, *515*, L464.
(4) Yarovsky, I.; Spencer, M. J. S.; Nelson, S.; Snook, I., to be published elsewhere.
(5) Spencer, M. J. S.; Hung, A.; Snook, I.; Yarovsky, I. *Surf. Sci.* **2003**, *540*, 420.
(6) Buckley, D. H. *Int. J. Nondestr. Test.* **1970**, *2*, 171.
(7) Rose, J. H.; Smith, J. R.; Ferrante, J. *Phys. Rev. B: Condens. Matter* **1983**, *28*, 1835.
(8) Finnis, M. W. *J. Phys.: Condens. Matter* **1996**, *8*, 5811.
(9) Dupre, A. *Theorie Mechanique de la Chaleur*; Gauthier-Villars: Paris, 1869.
(10) Kresse, G.; Hafner, J. *Phys. Rev. B: Condens. Matter* **1993**, *48*, 13115.
(11) Kresse, G.; Furthmuller, J. *Comput. Mater. Sci.* **1996**, *6*, 15.
(12) Kresse, G.; Furthmuller, J. *Phys. Rev. B: Condens. Matter* **1996**, *54*, 11169.
(13) Kohn, W.; Sham, L. J. *Phys. Rev.* **1965**, *140*, 1133.
(14) Perdew, J. P.; Yue, W. *Phys. Rev. B: Condens. Matter* **1992**, *45*, 13244.
(15) Perdew, J. P.; Zunger, A. *Phys. Rev. B: Condens. Matter* **1981**, *23*, 5048.
(16) Monkhorst, H. J.; Pack, J. D. *Phys. Rev. B: Solid State* **1976**, *13*, 5188.
(17) Vanderbilt, D. *Phys. Rev. B: Condens. Matter* **1990**, *41*, 7892.
(18) Spencer, M. J. S.; Hung, A.; Snook, I. K.; Yarovsky, I. *Surf. Sci.* **2002**, *513*, 389.
(19) Spencer, M. J. S.; Hung, A.; Snook, I.; Yarovsky, I. *Surf. Rev. Lett.* **2003**, *10*, 169.
(20) Muscat, J.; Hung, A.; Russo, S.; Yarovsky, I. *Phys. Rev. B: Condens. Matter* **2002**, *65*, 054107/1.
(21) Hung, A.; Muscat, J.; Yarovsky, I.; Russo, S. P. *Surf. Sci.* **2002**, *520*, 111.
(22) Hung, A.; Muscat, J.; Yarovsky, I.; Russo, S. P. *Surf. Sci.* **2002**, *513*, 511.
(23) Methfessel, M.; Paxton, A. T. *Phys. Rev. B: Condens. Matter* **1989**, *40*, 3616.
(24) Blochl, P. E.; Jepsen, O.; Andersen, O. K. *Phys. Rev. B: Condens. Matter* **1994**, *49*, 16223.
(25) Finklea, S. L.; Cathey, L.; Amma, E. L. *Acta Crystallogr., Sect. A* **1976**, *32*, 529.
(26) Buerger, M. J. *Am. Mineral.* **1931**, *16*, 361.
(27) Mikhlin, Y. L.; Tornashevich, Y. V.; Pashkov, G. L.; Okotrub, A. V.; Asanov, I. P.; Mazalov, L. N. *Appl. Surf. Sci.* **1998**, *125*, 73.